Response of Photonic Hydrogels of Homogeneous Particles to Uranyl Ions in Aqueous Solutions

R. G. JOSHI[1*], Deepak K. GUPTA[1], P. AMESH[2], P. K. PARIDA[3], and T. R. RAVINDRAN[1]

[1]*Materials Science Group, Indira Gandhi Centre for Atomic Research, A CI of Homi Bhabha National Institute, Kalpakkam 603102, India*

[2]*Materials Chemistry and Metal Fuel Cycle Group, Indira Gandhi Centre for Atomic Research, A CI of Homi Bhabha National Institute, Kalpakkam 603102, India*

[3]*Metallurgy and Materials Group, Indira Gandhi Centre for Atomic Research, A CI of Homi Bhabha National Institute (HBNI), Kalpakkam 603102, India*

[*]Corresponding author: R. G. JOSHI E-mail: rgjoshi@igcar.gov.in

Abstract: We study here the response of photonic hydrogels (PHs), made of photonic crystals of homogeneous silica particles in polyacrylamide hydrogels (SPHs), to the uranyl ions UO_2^{2+} in aqueous solutions. It is found that the reflection spectra of the SPH show a peak due to the Bragg diffraction, which exhibits a blue shift in the presence of UO_2^{2+}. Upon exposure to the SPH, UO_2^{2+} gets adsorbed on the SPH and forms complex coordinate bonds with multiple ligands on the SPH, which causes shrinking of hydrogel and leads to the blue shift in the diffraction peak. The amount of the blue shift in the diffraction peak increases monotonically up to UO_2^{2+} concentrations as high as 2300 μM. The equilibration time for the shift in the Bragg peak upon exposure to UO_2^{2+} is found to be ~30 min. These results are in contrast to the earlier reports on photonic hydrogels of inhomogeneous microgel particles hydrogel (MPH), which shows the threshold UO_2^{2+} concentration of ~600 μM, below which the diffraction peak exhibits a blue shift and a change to a red shift above it. The equilibration time for MPH is ~300 min. The observed monotonic blue shift and the faster time response of the SPH to UO_2^{2+} as compared to the MPH are explained in terms of homogeneous nature of silica particles in the SPH, against the porous and polymeric nature of microgels in the MPH. We also study the extraction of UO_2^{2+} from aqueous solutions using the SPH. The extraction capacity estimated by the arsenazo-III analysis is found to be 112 mM/kg.

Keywords: Photonic hydrogels; uranium extraction and monitoring; arsenazo-III-uranium complex; polyacrylamide hydrogel; UV-visible spectroscopy

Citation: R. G. JOSHI, Deepak K. GUPTA, P. AMESH, P. K. PARIDA, and T. R. RAVINDRAN, "Response of Photonic Hydrogels of Homogeneous Particles to Uranyl Ions in Aqueous Solutions," *Photonic Sensors*, 2023, 13(4): 230417.

1. Introduction

The photonic hydrogel (PH) consists of a photonic crystal incorporated into a polymeric hydrogel matrix [1–8]. To obtain a PH, a photonic crystal is prepared by self-assembly [2, 9, 10] of monodisperse colloidal particles in a gelation medium which is then gelled by the polymerization process like photopolymerization [7, 8, 11, 12], therefore, it is also called a portable photonic crystal.

Received: 11 May 2023 / Revised: 6 July 2023

DOI: 10.1007/s13320-023-0695-8
Article type: Regular

The PH possesses the optical properties of a photonic crystal to inhibit the propagation of certain wavelengths of light satisfying the Bragg diffraction condition [2, 7, 8, 13], thereby giving rise to optical stop bands at those wavelengths. The PH also possesses the properties of hydrogels to swell/ deswell in response to the change in its environmental conditions [1, 12, 14]. Swelling/deswelling of the PH is associated with the expansion/contraction of the embedded photonic crystal lattice, resulting in a corresponding change in its optical properties. Thus, monitoring the change in the optical properties of the PH provides a way to monitor the changes in its environmental/solvent conditions. There are several reports demonstrating the utilization of PHs for the development of sensors for pH, temperature, ionic strength, glucose, chemicals [1, 2, 5, 8, 14–19], etc., as well as for the development of optical devices [3, 13, 20].

Uranium extraction from aqueous solutions (sea water/nuclear industrial waste) is of high importance to reduce the contamination of the solvents and recycle nuclear fuel [21–23]. In an aqueous solution, uranium exists in the form of uranyl ions (UO_2^{2+}) as the most stable form. Several materials based on nanoparticles, hydrogels, and metal-organic frameworks have been reported to extract UO_2^{2+} by adsorption [24–30]. For example, poly acrylic acid hydrogels are found to have the good efficiency in removing UO_2^{2+} from the waste water with a high adsorption capacity of 445.1 mg/g [24]. MCM-41 silica particles grafted with polyacrylonitrile and further modified with carboxyl groups have also shown a high adsorption capacity of 442.3 mg/g [25]. The hydrogel-like spidroin-based protein fiber is shown to be ultrafast and highly selective in the extraction of UO_2^{2+} from sea water with the extraction capacity of 12.33 mg/g [29]. Magnetic nanoparticles functionalized with phosphate-based complex coating are reported to have the excellent selectivity and adsorption capacity (1690 mg/g) [30] as well as offer an advantage for easy collection and removal from the solvent using a magnetic field.

While the above materials are good for the extraction of UO_2^{2+} from aqueous solutions, they cannot be analyzed directly to investigate the amount of uranium extracted/adsorbed. The analysis of the extracted uranium is performed using the solvent remaining after extraction with the help of some other techniques like fluorescence [31–33], radiochemical methods [34], alpha spectrometry [35], and inductively coupled plasma mass spectrometry [36]. Byrne *et al*. [34] have used the radiochemical neutron activation analysis method to determine uranium levels in blood, hair, and urine of occupationally exposed persons. Wang *et al*. [33] have developed a resonance fluorescence chemosensor for the determination of uranium (VI) based on the formation of the heterobinuclear complex with europium (III) and a di-tetradentate macrocyclic ligand. Although these techniques are reasonably sensitive and effective, they need expensive and complicated instrumentation, making it difficult to perform onsite characterization. However, colorimetric techniques [37–39] facilitate the onsite characterization of uranium due to the portability of instruments. Colorimetric sensors exhibit the change in color upon exposure to uranium and hence offer an advantage of qualitative detection of uranium in the solution just by visual observation [37, 40]. In order to analyze uranium, all the above techniques need pre-processing of the solvent, which further delays the analysis after extraction and thus, real time (in situ) information about extracted uranium is lacking with these techniques.

On the other hand, recently Joshi *et al*. [41] have reported a microgel based PH which has a good extraction capacity (487 mM/kg) for UO_2^{2+} in aqueous solutions. Joshi *et al*. [41] have referred to the microgel based PHs as composite photonic crystals (CPC); to be more specific, we have re-named it as microgel particles hydrogel (MPH). During extraction, the MPH shows a shift in its

diffraction peak upon adsorption of UO_2^{2+}, enabling its real time monitoring. However, the shift in the diffraction of MPH with respect to the change in the UO_2^{2+} concentration is not monotonic. The MPH has a threshold for UO_2^{2+} at ~600 μM, below which the diffraction peak exhibits a blue shift and a change to a red shift above the threshold [41], making it difficult to correlate the shift in the diffraction peak with the associated UO_2^{2+} concentration. The response of the MPH to UO_2^{2+} is also found to be quite slow. It takes about 300 min to reach the equilibrium for the shift in the diffraction peak or extraction of UO_2^{2+}. Here, we report studies on PHs, prepared using homogeneous silica particles in polyacrylamide hydrogels (SPHs), which exhibits monotonic blue shift in its diffraction peak and has faster response compared to the MPH. Xiao *et al.* [42] have reported studies on the extraction and monitoring of uranium using a silica based PH. However, Xiao *et al.* [42] have monitored the Bragg shift in the SPH with respect to uranium up to the concentration of 300 μM, whereas the threshold uranium concentration in the case of MPH is found to be ~600 μM. Also, Xiao *et al.* [42] performed the measurement after 12-hour exposure of the SPH to uranium and time dependent evolution of shift in Bragg diffraction peak upon the exposure was not reported. Thus, it is not known if there is any threshold uranium concentration for the shift in the Bragg peak in the case of the SPH as observed in the case of the MPH and, what is the time required for the shift in the Bragg peak in the SPH to reach the equilibrium upon exposure to uranium. Here, we report detailed studies on the evolution of the Bragg diffraction peak of the SPH with respect to the uranium concentration as high as 2300 μM and as a function of time after exposure to uranium. Our studies reveal that the SPH exhibits the monotonic blue shift in the diffraction peak up to the uranium concentration of 2300 μM and has about 10 times faster time response (30 sec) compared to the MPH. Studies on the extraction capacity of the SPH (analyzed from absorption spectra of uranium-arsenazo-III complexes) for UO_2^{2+} are also presented. The results of the SPH are discussed in light of the homogeneous nature of silica particles in contrast to the inhomogeoeous/polymeric nature of microgels in the MPH.

2. Materials and methods

2.1 Synthesis of silica particles

Silica particles are synthesized using well known Stöber's method [43, 44]. This silica particle suspension is purified by dialysis against milli-*Q* water for a few days and concentrated by centrifugation. Concentrated suspensions are kept in contact with ion exchange resigns (bio-rad) for further de-ionization. After a few hours of de-ionization, concentrated suspensions develop iridescence, indicating the ordering of silica particles in a crystalline state. The radius and polydispersity of silica particles, characterized using dynamic light scattering, are found to be 117 nm and 5%, respectively.

2.2 Preparation of SPHs

SPHs are prepared by incorporating the homogeneous silica particles photonic crystal in a polyacrylamide hydrogel matrix [4, 6, 7]. In the case of the MPH, the use of microgels (which are porous and inhomogeneous) leads to interpenetration/entanglements of polymer chains of the microgel and hydrogel giving rise to complex interactions [8], which are responsible for the slow and nonmonotonic response of the MPH towards UO_2^{2+}. In the SPH, due to the presence of homogeneous silica particles, such complex interactions with hydrogel are absent, and hence, it is expected to show the improved response for uranyl ions. Towards this, stock solutions of acrylamide (6 M) and N,N′-methylene bis-acrylamide (0.25 M) are prepared in the milli-*Q* water. Silica photonic crystals are prepared in the pregel medium by adding 200 μL of acrylamide

solution (6 M) and 400 μL of N,N′-methylene bis-acrylamide solution (0.25 M) to 1.4 mL of the above concentrated silica suspension. Then, 2 μL of photo-initiator (diethoxy acetophenone-DEAP) is added, and the reaction mixture is kept in contact with mixed-bed resins till the iridescence appears. The silica photonic crystal in the pregel solution is injected into a cell formed with two quartz slides (1 mm thick) separated by the 250 μm spacer (two layers of 125 μm parafilm) and exposed to the ultra violet (UV) radiation (325 nm lamp) for 1 hour. Exposure to UV leads to the formation of polyacrylamide hydrogel around the silica particles which fixes the photonic crystal into hydrogel and develops as an SPH. The SPH is isolated from the cell and soaked in milli-Q water for 48 hours for purification and equilibration before subjecting to UV-visible characterization. A piece of purified SPH is dried at the room temperature (23 ℃) for 48 hours and gold coated for scanning electron microscopy (SEM) imaging [Fig. 1(a)]. The SEM image shows silica particles ordered in arrays embedded in the polyacrylamide matrix.

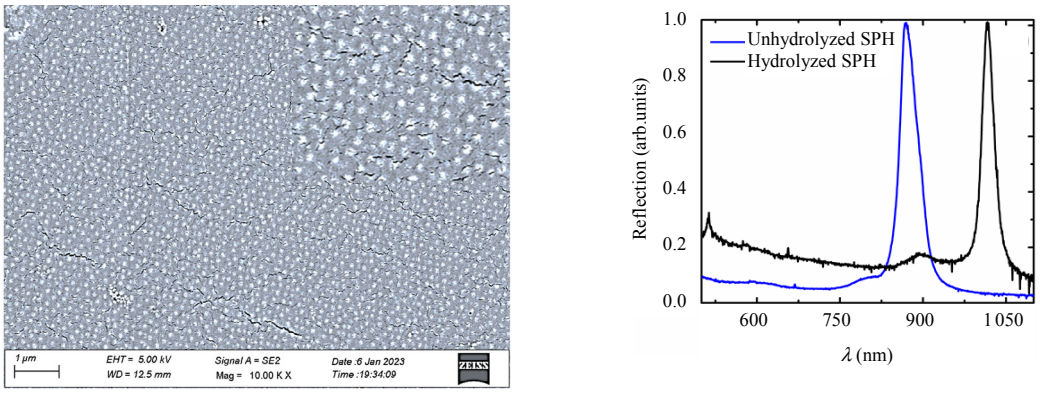

(a) (b)

Fig. 1 Characterization of ordering of silica particles in the SPH: (a) SEM image of the dried SPH showing ordered arrays of silica particles embedded in polyacrylamide. Inset shows the magnified SEM image of the dried SPH and (b) normalized UV-visible reflection spectra of un-hydrolyzed and hydrolyzed SPH (color online).

3. Results and discussion

3.1 Investigations on response of the SPH to UO_2^{2+}

The response of the SPH to UO_2^{2+} with respect to the time as well as the concentration is characterized by recording its corresponding UV-visible spectra. All spectra are recorded using the fiber-based UV-visible spectrometer (Avantes, Netherlands) under normal incidence at the room temperature. Figure 1(b) shows the reflection spectra for the as-prepared SPH. It shows a peak at ~880 nm. The peak occurs due to the Bragg diffraction of light from the silica photonic crystal at a wavelength where the diffraction condition $2\mu d_{hkl} = n\lambda$ is satisfied. Here, d_{hkl} is the interplaner spacing of the SPH, μ is the refractive index of the solvent, and n is the order of diffraction. For the as-prepared SPH, the near-neighbour separation, d_{nn}, can be determined from the peak position, λ_{peak} using the relation [45], $d_{nn} = \sqrt{3/2}\left(\lambda_{peak}/2\mu\right)$ and is found to be 405 nm. The lattice constant estimated using the relation for a face centred cubic structure [46, 47], $a = \sqrt{2}d_{nn}$ is found to be 573 nm. The as-prepared SPH has amide ($-NH_2$) ligands from polyacrylamide to capture the UO_2^{2+}. However, it is known that carboxyl groups ($-COOH$) are highly efficient ligands to extract UO_2^{2+} compared to amide groups [24]. In order to convert the existing amide groups of the SPH into carboxyl groups, the SPH is subjected to hydrolysis in an aqueous solution of 0.5 M NaOH for 3 hours. Carboxyl groups dissociate in the aqueous medium and add charges to polymer chains; as a result, the hydrogel swells due to columbic repulsion of charges on polymer chains.

Indeed, we see in Fig. 1(b) a red shift in the Bragg diffraction peak for the hydrolyzed SPH, which arises from the expansion of the photonic crystal lattice due to swelling of hydrogel upon hydrolysis and thus confirms the conversion of amide groups into carboxyl groups. Along with the red shift, the spectral bandwidth of the hydrolyzed sample is seen to decrease as compared to the unhydrolyzed one. This is due to the corresponding change in the crystallite size of photonic crystals embedded in the SPH. As the SPH swells/expands upon hydrolysis, the crystallite size increases resulting in a reduction of the spectral width. Swelling of the SPH is also expected to improve its time response for uranium due to the increased pore size/enhanced solvent diffusion. Upon hydrolysis for more than 3 hours, the SPH is found to become fragile and difficult to handle. The 3 hours hydrolyzed SPH is cut into pieces of the size ~10 mm × 10 mm and used for all further measurements. Uranium solutions with different concentrations are prepared from the uranyl nitrate stock solution (144 mM in 1 M nitric acid) by its dilution. The carboxylic group shows the maximum extraction efficiency for uranium at pH (~5.5) [24], therefore, all the uranium solutions are prepared at pH (~5.5) using the 0.1 M acetate buffer.

3.1.1 Time dependence

The time response of the SPH to UO_2^{2+} is studied by monitoring the time evolution of its Bragg peak in the presence of UO_2^{2+}. For this purpose, the SPH is soaked into the 75 μM UO_2^{2+} solution and its reflection spectra are recorded as a function of time after soaking, directly from the container using the fiber optical probe [Fig. 2(a)]. The spectra show the Bragg peak which undergoes a blue shift at the initial time and reaches saturation at the later time. Figure 2(b) shows the peak position with respect to the time after soaking. It is seen that the shift in the Bragg peak reaches saturation in about 30 min from soaking. Along with the shift, the shape of the reflection spectra of the SPH is also found to vary upon the adsorption of uranyl ions due to the polycrystalline nature of the photonic crystal embedded in the SPH. As the SPH shrinks upon adsorption of uranyl ions, the size of the crystallites decreases, resulting in broadening of the peak in the spectra. In addition to this, spectra at higher uranyl ion concentrations show multiple peaks due to the non-homogeneous shrinking of hydrogel resulting from the non-homogeneous crosslinking of hydrogel in photopolymerization. The blue shift in the peak results from adsorption of UO_2^{2+} on the SPH (discussed in detail in a later section). Therefore, saturation in shifting of the peak position also indicates that the saturation/equilibrium time for adsorption of UO_2^{2+} on the SPH is ~30 min. In the case of the MPH, the saturation time for shifting of the Bragg peak/adsorption of UO_2^{2+} has found to be ~300 min, which is 10 times larger than the time observed for the SPH. It suggests that the SPH has relatively rapid response towards adsorption of UO_2^{2+} as compared to the MPH. The slow response from the MPH could be due to the complex nature of interactions between microgel and hydrogel arising from interpenetrating networks of polymer chains between the microgel and hydrogel [8, 12]. The porous and polymeric nature of microgels [48] leads to the formation of the interpenetrating network of polymer chains between the microgels and hydrogel, which induces additional crosslinks (physical) between the polymer chains. The MPH also has the relatively high polymer content as a contribution from microgels as well as a hydrogel. On the other hand, silica particles in the SPH are non-porous (homogeneous), which are simply grafted in polyacrylamide chains. The SPH has the relatively low polymer content as the polymer contribution comes only from the hydrogel. Also in the hydrolyzed SPH, negative charges are present in a large amount all over the hydrogel, which impart electrostatic attraction to UO_2^{2+}, whereas in the MPH charges are present in a small amount only on

the microgel, and the hydrogel as such is neutral. Due to these conditions, the SPH has relatively rapid response for UO_2^{2+} compared to the MPH. At higher concentrations of UO_2^{2+}, the time response of the SPH is found to be even faster. However, in order to keep the same time scales based on above studies, the measurements are carried out after one hour of soaking for all concentrations of UO_2^{2+}.

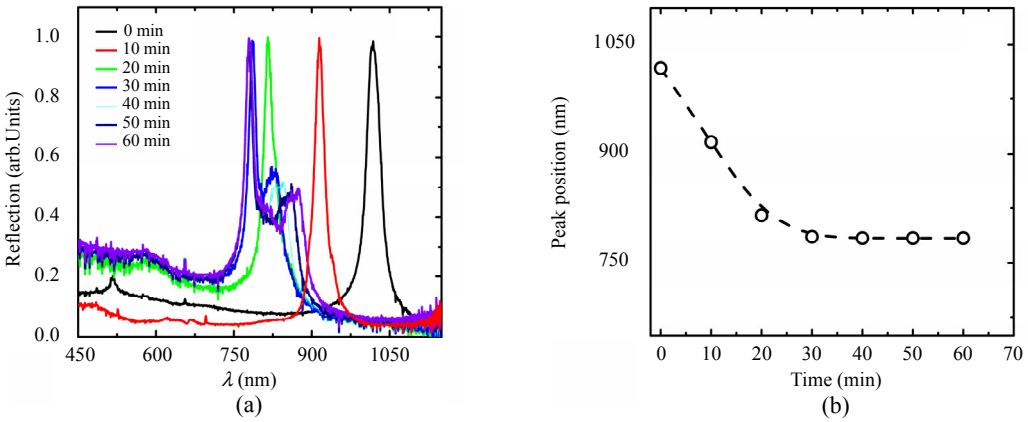

Fig. 2 Time response of the SPH to uranyl ions: (a) normalized UV-visible reflection spectra and (b) corresponding diffraction peak positions of the SPH as a function of the time after soaking into the 75 μM uranyl ions solution. The dashed line is the guide to the eye (color online).

3.1.2 Explanation for blue shift in Bragg diffraction peak of the SPH

The observed blue shift in the Bragg diffraction peak of the SPH upon adsorption of UO_2^{2+} can be explained by considering the chelation interactions (complex coordinate formation) between uranyl ions and carboxyl ligands present on hydrogel polymer chains [24]. An evidence for the formation of the complex coordinates between uranyl ions and carboxyl ligands has been reported in the literature through (infrared radiation) IR/Raman spectroscopic measurement [42, 49, 50]. The UO_2^{2+} ions have the ability to form complex coordinates with multiple ligands. As multiple ligands approach towards single uranyl ion for chelation, polymer chains to which ligands are attached also get pulled together resulting in deswelling (shrinking) of the SPH. Figure 3 shows the schematic diagram for the deswelling (shrinking) of the SPH upon adsorption of UO_2^{2+}. In the SPH, the silica photonic crystal is embedded into the hydrogel, therefore shrinking of the SPH causes shrinking of inter-planar spacing of the silica photonic crystal, which is responsible for the blue shift in the Bragg diffraction peak observed in the reflection spectra. Shrinking of the SPH upon exposure to UO_2^{2+} ions is also evident from the photographs (Fig. 4). The photographs are taken under the white light illumination. As seen from the photograph, the SPHs show colours due to the diffraction, which is prominent in the shrunken SPH (after adsorption of uranyl ions at the higher concentration), as its reflection peak lies in the visible region [Fig. 5(a)]. The colors are faint due to weak diffraction by SPHs, as apparent from the weak and broad diffraction peak in the reflection spectra recorded at higher concentrations of UO_2^{2+} [Fig. 5(a)].

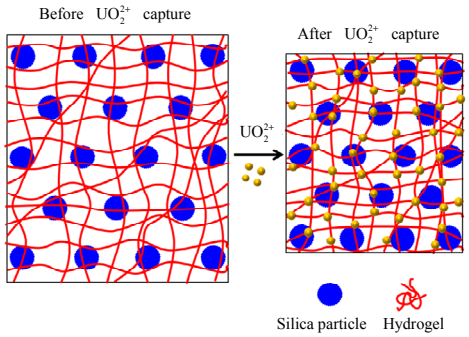

Fig. 3 Schematic diagram showing shrinking (de-swelling) of the SPH upon capturing UO_2^{2+} ions (color online).

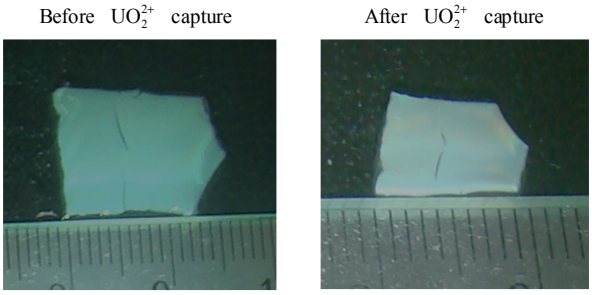

Fig. 4 Photographs of the SPH before and after extraction of uranyl ions.

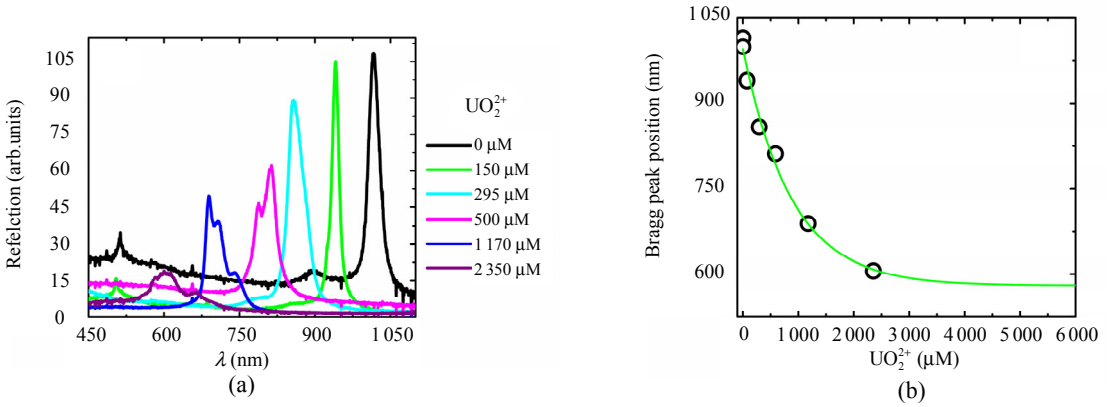

Fig. 5 Response of the SPH to change in the uranyl ion concentration: (a) recorded UV-visible reflection spectra and (b) corresponding diffraction peak positions of the SPH at different UO_2^{2+} concentrations in aqueous solutions. The continuous line is the fit of the experimental data to (1) extrapolated to show saturation at the higher concentrations (color online).

3.1.3 Concentration dependence

To study the dependence of the shift in the Bragg peak position on the UO_2^{2+} concentration, pieces of the SPH are soaked in different concentrations of UO_2^{2+}. Reflection spectra of the SPH at different values of UO_2^{2+} are shown in Fig. 5(a). With increasing UO_2^{2+}, the diffraction peak gets broadened and its intensity decreases. This is due to a decrease in the size of the crystallites resulting from the shrinking of the SPH upon adsorption of uranyl ions. The multiple peaks in spectra at higher UO_2^{2+} concentrations are due to inhomogeneous shrinking, arising from inhomogeneous crosslinking density of the photo-polymerized SPH. Moreover, all spectra show a blue-shifted Bragg peak. As seen from Fig. 5(b), the extent of the blue shift increases monotonically with an increase in UO_2^{2+}. This is in contrast with the MPH that is found to have a threshold concentration for UO_2^{2+}, below which the diffraction peak exhibits a blue shift and a change to a red shift above it [41] . This can be understood in the following way: the diffusion of UO_2^{2+} into a PH upon its immersion in a UO_2^{2+} solution has two counteracting effects. One is the binding of UO_2^{2+} with multiple ligands (ionic crosslinking) by the formation of complex coordinates which can cause shrinking of a PH [51]. The other effect is that it increases the mixing contribution to the osmotic pressure inside a PH, which can cause swelling of a PH [52]. For complex coordinates formation, most of the ligands in the hydrolyzed SPH are carboxyl groups, whereas in the case of the MPH, the majority of the ligands are of amide groups (NH_2 – from the polyacrylamide hydrogel and NH – from

the poly N-isopropylacrylamide-co-poly acrylic acid microgel) and a small amount of carboxyl groups from acrylic acid (present in microgels) [41]. It is known that the carboxyl groups have higher binding affinity towards uranyl ions than amide groups [24, 53]. Therefore, in the SPH, the effect of binding of UO_2^{2+} to carboxylate ions dominates the mixing contribution at all studied concentrations, giving rise to continuous shrinking of the SPH (a blue shift in the diffraction peak). On the other hand, in the MPH, the binding contribution dominates over mixing in the low concentration regime where the MPH exhibits shrinking (a blue shift in the diffraction peak) and the mixing contribution dominates over binding in the high concentration regime making the MPH swell (a red shift in the diffraction peak), giving rise to the threshold behavior. This explains the observed monotonic blue shift in the diffraction peak for the SPH and the threshold behavior for the MPH with the increasing UO_2^{2+} up to concentrations as high as 2300 μM. The shift in the reflection peak during an increase in the concentration of UO_2^{2+} is expected to saturate when all the ligands available on the SPH to adsorb UO_2^{2+} are exhausted. Since the diffraction peak intensity is found to become weaker with increasing UO_2^{2+} concentration [Fig. 5(a)], the UO_2^{2+} concentration for the saturation of the reflection peak could not be measured experimentally. The concentrations of UO_2^{2+} for the saturation of the shift can be predicted by extrapolating the experimentally observed behavior of the peak wavelength with the UO_2^{2+} concentration. The shift in the peak of the SPH occurs due to a decrease in the inter-planar spacing of the photonic crystal (as given by the Bragg condition $2\mu d_{\text{hkl}}\sin\theta = \lambda_{\text{peak}}$), which in turn arises from the deswelling of the hydrogel containing it. Since the deswelling of the hydrogel can be described by exponential dependence [52], we apply the same here to describe the shift in the peak wavelength as the following:

$$\lambda_{\text{peak}}(UO_2^{2+}) = \lambda_{\text{peak\_s}} + D\exp\left(-\frac{UO_2^{2+}}{K}\right) \quad (1)$$

where $\lambda_{\text{peak}}(UO_2^{2+})$ is the peak wavelength at a given UO_2^{2+} concentration, $\lambda_{\text{peak\_s}}$ is the saturated peak wavelength, D is the amplitude of the shift, and K is a constant describing the inverse rate, at which the shift occurs. Using the above approach, we have fitted the dependence of the peak position on UO_2^{2+} concentrations [Fig. 5(b)] with (1), yielding the fitting parameters as $\lambda_{\text{peak\_s}}$ =579.3 nm, D=416.7 nm, and K=877.1 μM. Extrapolation of the peak wavelength to higher uranium concentrations suggests that the saturation in the shift in the reflection peak will occur at ~4500 μM.

We have also investigated the response of the SPH to other divalent as well as monovalent ions. For this purpose, pieces of the SPH are soaked in solutions of different ions (Mg^{2+}, Ni^{2+}, Fe^{2+}, and K^+) with the concentration of 500 μM each at pH (~5.5) and the corresponding reflection spectra are recorded after one hour of adsorption (Fig. 6). For reference, spectra of the SPH exposed to 500 μM UO_2^{2+} and without exposing to any ions are also shown. Figure 6 shows that the blue shift for UO_2^{2+} ions is much larger than that for other divalent or monovalent ions. The larger blue shift for UO_2^{2+} may result from its larger size, so it can coordinate with more number of ligands as compared to other ions [23, 54].

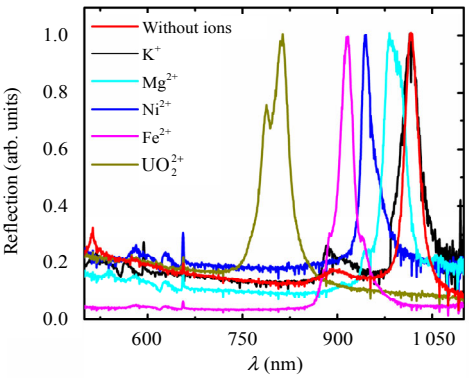

Fig. 6 Normalized UV-visible reflection spectra of the SPH upon adsorption of different ions (color online).

3.2 Extraction of UO_2^{2+} from aqueous solutions using the SPH

We also estimate the extraction capacity of the SPH for UO_2^{2+}. For this purpose, 0.002 g (dried) of the SPH is soaked in 5 mL of 300 µM of the UO_2^{2+} solution at a pH (~5.5) for 1 hour. UO_2^{2+} extracted by the SPH is estimated using the arsenazo-III dye analysis [41, 55]. In this analysis, the uranium solution (250 µL) is mixed with 10 M HNO_3 (3 mL) in the presence of aqueous solutions of arsenazo-III dye (250 µL, 0.1 wt.%) and sulphamic acid (250 µL, 10%) and finally the volume of the mixture is made 5 mL by adding 10 M HNO_3. The mixture is kept for 2 hours undisturbed for uranium-arsenazo-III complex formation and then analyzed using UV-visible absorption spectra. The samples are prepared from the 300 µM uranium solution before and after the extraction in this solution by the SPH. Figure 7 shows the absorption spectra for uranium-arsenazo-III mixtures prepared before and after the extraction. A peak at ~650 nm in both spectra confirms the formation of uranium-arsenazo-III complexes. The intensity of the peak at ~650 nm depends upon the amount of UO_2^{2+} in the solution. As expected, the absorption peak is more intense for the solution before extraction as compared to that after extraction. The extraction efficiency (E) of the SPH can be determined from absorption data using the following relation, $E = \frac{(A_i - A_f)}{A_i}\% = \frac{(C_i - C_f)}{C_i}\%$, where A_i and A_f are initial and final absorptions, and C_i and C_f are corresponding concentrations, respectively. The analysis shows that the SPH has the extraction efficiency of ~25%. We also estimate the adsorption capacity of the SPH using the relation, $Q = \frac{(C_i - C_f)}{m} V\%$, where V is the volume of the solution and m is the mass of the SPH, and find it to be 44 mg/g or 112 mM/kg of the SPH. The Q value for the present SPH is higher than that reported by Xiao *et al.* [42] (~58 mM/kg), which could be due to the use of the longer hydrolysis time (3 hours) and high BIS content (0.8 wt%). The Q value of the SPH is comparable to or better than that reported for some of the other materials, e.g., Fe_3O_4-halloysite nanotube (88.32 mg/g) [26], thermo-sensitive hydrogel (14.69 mg/g) [53], and hydrogel like spidroin-based protein fiber (12.33 mg/g) [29]. However, the extraction capacity for the SPH (112 mM/kg) is less than that for the MPH (487 mM/kg) [41], which is due to the low polymer content of the SPH as compared to the MPH. In the SPH, only the hydrogel contributes to the polymer content, whereas in the MPH, the hydrogel plus microgel contribute to the polymer content. As a result, the number of ligands available for capturing UO_2^{2+} is more in the MPH than in the SPH, giving a higher extraction capacity for the MPH. The uranium extracted by the SPH can be separated by soaking the SPH in a strong acid solution, as the interaction between ligand groups (carboxyl and amide) and UO_2^{2+} is expected to get weakened in the acidic medium due to the protonation of ligands, and then the regenerated SPH can be recycled for extraction of uranium. As reported by Xiao *et al.* [42], the uranium extracted by the SPH can be separated using the 1 M HCl solution and the regenerated SPH can be recycled 6 times for extraction with the recovery efficiency over 94.75%.

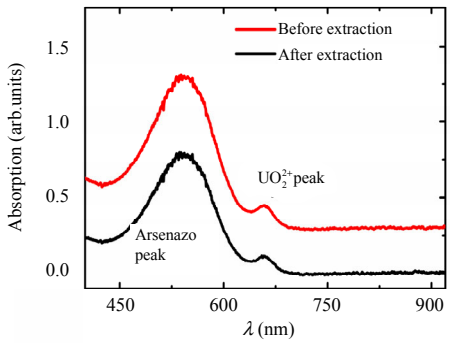

Fig. 7 UV-visible absorption spectra of uranyl ion-arsenazo-III complex before and after extraction of UO_2^{2+} in aqueous solutions (color online).

4. Summary and conclusions

We have presented a novel SPH and studied its response to uranyl ions in aqueous solutions. It is found that the SPH exhibits a blue shift upon capture of uranium by adsorption. The SPHs respond quite faster to UO_2^{2+}, i.e., taking only ~30 min. to reach equilibrium in adsorption of UO_2^{2+} /in time evolution of its Bragg peak. The blue shift increases monotonically with an increase in the UO_2^{2+} concentration. The fast response and monotonic blue shift in the Bragg peak observed in the SPH offer the advantage over the MPH, as the MPH has ten times slower response (taking ~300 min. to reach equilibrium in UO_2^{2+} adsorption) and exhibits a threshold behavior. The extraction efficiency of the SPH is found to be 112 mM/kg, which is, however, lower than that of the MPH (487 mM/kg). The homogeneous nature of silica particles in the SPH against the inhomogeneous/polymeric nature of microgels in the MPH is responsible for the faster and monotonic response, but the low extraction capacity of the SPH for UO_2^{2+} over the MPH. We believe that our work will motivate further research on PHs towards their utilization for fast and accurate detection/extraction of uranium and other heavy metal ions with the enhanced extraction capacity.

Acknowledgment

We thank Dr. K. A. VENKATESAN for technical discussions. We also thank Dr. B. VENKATRAMAN, Dr. R. DIWAKAR, Dr. N. V. CHANDRASHEKAR and Dr. Awadhesh MANI for their support and encouragement.

Declarations

Conflict of Interest The authors declare that they have no competing interests.

References

[1] S. A. Asher and J. H. Holtz, "Polymerized colloidal crystal hydrogel films as intelligent chemical sensing materials," *Nature*, 1997, 389(6653): 829–832.

[2] J. M. Weissman, H. B. Sunkara, A. S. Tse, and S. A. Asher, "Thermally switchable periodicities and diffraction from mesoscopically ordered materials," *Science*, 1996, 274(5289): 959–963.

[3] C. E. Reese, A. V Mikhonin, M. Kamenjicki, A. Tikhonov, and S. A. Asher, "Nanogel nanosecond photonic crystal optical switching," *Journal of American Chemical Society*, 2004, 126(5): 1493–1496.

[4] A. Toyotama, J. Yamanaka, M. Shinohara, S. Onda, T. Sawada, M. Yonese, *et al.*, "Gel immobilization of centimeter-sized and uniform colloidal crystals formed under temperature gradient," *Langmuir*, 2009, 25(1): 589–593.

[5] T. Kanai, N. Kobayashi, and H. Tajima, "Enhanced linear thermosensitivity of gel-immobilized colloidal photonic crystal film bound on glass substrate," *Materials Advances*, 2021, 2(8): 2600–2603.

[6] Y. Iwasawa, H. Tajima, and T. Kanai, "Tuning and fixing of uniform Bragg reflection color of gel-immobilized colloidal photonic crystal films," *Polymer Journal*, 2021, 53(10): 1157–1161.

[7] T. Kanai, T. Sawada, and J. Yamanaka, "Fabrication of large-area silica colloidal crystals immobilized in hydrogel film," *Journal of the Ceramic Society of Japan*, 2010, 118(1377): 370–373.

[8] R. G. Joshi, D. Karthickeyan, D. K. Gupta, and B. V. R. Tata, "Effect of entanglements on temperature response of gel immobilized microgel photonic crystals," *Colloids and Surfaces A: Physicochemical and Engineering Aspects*, 2018, 558: 600–607.

[9] B. V. R. Tata, R. G. Joshi, D. K. Gupta, J. Brijitta, and B. Raj, "Crystalline arrays of submicron-sized particles through colloidal route," *Current Science*, 2012, 103(10): 1175–1184.

[10] P. Liu, L. Bai, J. Yang, H. Gu, Q. Zhong, Z. Xie, *et al.*, "Self-assembled colloidal arrays for structural color," *Nanoscale Advances*, 2019,1(5): 1672–1685.

[11] J. M. Weissman, H. B. Sunkara, A. S. Tse, and S. A. Asher, "Thermally switchable periodicities and diffraction from mesoscopically ordered materials," *Science*, 1996, 274(5289): 959–963.

[12] W. Song, Y. Guan, Y. Zhang, and X. X. Zhu, "Mutual interaction between embedded microgel particles and the surrounding hydrogel matrix," *Soft Matter*, 2013, 9(9): 2629–2636.

[13] G. Pan, R. Kesavamoorthy, and S. A. Asher, "Optically nonlinear Bragg diffracting nanosecond optical switches," *Physical Review Letters*, 1997,

78(20): 3860–3863.

[14] M. Chen, L. Zhou, Y. Guan, and Y. Zhang, "Polymerized microgel colloidal crystals: photonic hydrogels with tunable band gaps and fast response rates," *Angewandte Chemie*, 2013, 125(38): 10145–10149.

[15] Z. Tang, S. Jia, L. Yao, Y. Guan, and Y. Zhang, "Inducing and erasing of defect state in polymerized microgel colloidal crystals via external stimuli," *Journal of Colloid Interface Science*, 2018, 526: 83–89.

[16] W. Cheng, J. Wang, U. Jonas, G. Fytas, and N. Stefanou, "Observation and tuning of hypersonic bandgaps in colloidal crystals," *Nature Materials*, 2006, 5(10): 830–836.

[17] S. Jia, Z. Tang, Y. Guan, and Y. Zhang, "Order-disorder transition in doped microgel colloidal crystals and its application for optical sensing," *ACS Applied Materials & Interfaces*, 2018, 10(17): 14254–14258.

[18] Y. Liu, Y. Zhang, and Y. Guan, "New polymerized crystalline colloidal array for glucose sensing," *Chemical Communications*, 2009, 14: 1867–1869.

[19] C. D. Geary, I. Zudans, A. V. Goponenko, S. A. Asher, and S. G. Weber, "Electrochemical investigation of Pb^{2+} binding and transport through a polymerized crystalline colloidal array hydrogel containing benzo-18-crown-6," *Analytical Chemistry*, 2005, 77(1): 185–192.

[20] K. T. Hufziger, S. V. Bykov, and S. A. Asher, "Raman hyperspectral imaging spectrometer utilizing crystalline colloidal array photonic crystal diffraction," *Applied Spectroscopy*, 2014, 68(11): 1219–1223.

[21] I. A. Katsoyiannis and A. I. Zouboulis, "Removal of uranium from contaminated drinking water: a mini review of available treatment methods," *Desalination and Water Treatment*, 2013, 51(13–15): 2915–2925.

[22] J. Kim, C. Tsouris, R. T. Mayes, Y. Oyola, T. Saito, C. J. Janke, *et al.*, "Recovery of uranium from seawater: a review of current status and future research needs," *Separation Science and Technology*, 2013, 48(3): 367–387.

[23] J. Wang and S. Zhuang, "Extraction and adsorption of U(VI) from aqueous solution using affinity ligand-based technologies: an overview," *Reviews in Environmental Science and Bio/Technology*, 2019, 18: 437–452.

[24] X. Yi, Z. Xu, Y. Liu, X. Guo, M. Ou, and X. Xu, "Highly efficient removal of uranium(VI) from wastewater by polyacrylic acid hydrogels," *RSC Advances*, 2017, 7(11): 6278–6287.

[25] G. Bayramoglu and M. Y. Arica, "MCM-41 silica particles grafted with polyacrylonitrile: modification in to amidoxime and carboxyl groups for enhanced uranium removal from aqueous medium," *Microporous and Mesoporous Materials*, 2016, 226: 117–124.

[26] W. He, Y. Chen, W. Zhang, C. Hu, J. Wang, and P. Wang, "Removal of UO_2^{2+} from aqueous solution using halloysite nanotube-Fe_3O_4 composite," *Korean Journal of Chemical Engineering*, 2016, 33: 170–177.

[27] W. Yang, Q. Pan, S. Song, and H. Zhang, "Metal-organic framework-based materials for the recovery of uranium from aqueous solutions," *Inorganic Chemistry Frontiers*, 2019, 6(8): 1924–1937.

[28] M. Carboni, C. W. Abney, S. Liu, and W. Lin, "Highly porous and stable metal-organic frameworks for uranium extraction," *Chemical Science*, 2013, 4(6): 2396–2402.

[29] Y. Yuan, Q. Yu, J. Wen, C. Li, Z. Guo, X. Wang, *et al.*, "Ultrafast and highly selective uranium extraction from seawater by hydrogel-like spidroin-based protein fiber," *Angewandte Chemie*, 2019, 131(34): 11911–11916.

[30] E. Calì, J. Qi, O. Preedy, S. Chen, D. Boldrin, W. R. Branford, *et al.*, "Functionalised magnetic nanoparticles for uranium adsorption with ultra-high capacity and selectivity," *Journal of Materials Chemistry A*, 2018, 6(7): 3063–3073.

[31] A. Kasdan, R. J. L. Chimenti, and J. P. DeNeufville, "Selective detection of uranium by laser-induced fluorescence: a potential remote-sensing technique 2: experimental assessment of the remote sensing of uranyl geologic targets," *Applied Optics,* 1981, 20(8): 1297–1307.

[32] N. Lin, R. Tao, Z. Chen, Q. Pan, Z. Zhu, B. Gao, *et al.*, "Design and fabrication of a new fluorescent film sensor towards uranyl ion via self-assembled monolayer," *Journal of Luminescence*, 2022, 242: 118562.

[33] J. Wang, X. Xiao, B. He, M. Jiang, C. Nie, Y. W. Lin, *et al.*, "A novel resonance fluorescence chemosensor based on the formation of heterobinuclear complex with a di-tetradentate macrocyclic ligand and europium (III) for the determination of uranium (VI)," *Sensors and Actuators B: Chemical*, 2018, 262: 359–364.

[34] A. R. Byrne and L. Benedik, "Uranium content of blood, urine and hair of exposed and non-exposed persons determined by radiochemical neutron activation analysis, with emphasis on quality control," *Science of Total Environment*, 1991, 107: 143–157.

[35] C. L. Duarte and M. S. M. F. Szeles, "An improved method for determination of uranium isotopic composition in urine by alpha spectrometry," *Journal of Radioanalytical and Nuclear Chemistry*, 1994, 177(1): 73–79.

[36] A. Lorber, Z. Karpas, and L. Halicz, "Flow injection

method for determination of uranium in urine and serum by inductively coupled plasma mass spectrometry," *Analytica Chimica Acta*, 1996, 334(3): 295–301.

[37] V. V. Halali and R. G. Balakrishna, "An expeditious method for the ultra-level chemosensing of uranyl ions," *Analytical Methods*, 2020, 12(8): 1070–1076.

[38] Y. Luo, Y. Zhang, L. Xu, L. Wang, G. Wen, A. Liang, *et al.*, "Colorimetric sensing of trace UO_2^{2+} by using nanogold-seeded nucleation amplification and label-free DNAzyme cleavage reaction," *Analyst*, 2012, 137(8): 1866–1871.

[39] W. Yun, H. Wu, X. Liu, H. Zhong, M. Fu, L. Yang, *et al.*, "Ultra-sensitive fluorescent and colorimetric detection of UO_2^{2+} based on dual enzyme-free amplification strategies," *Sensors and Actuators B: Chemical*, 2018, 255: 1920–1926.

[40] X. Cheng, X. Yu, L. Chen, H. Zhang, Y. Wu, and F. Fu, "Visual detection of ultra-trace levels of uranyl ions using magnetic bead-based DNAzyme recognition in combination with rolling circle amplification," *Microchimica Acta*, 2017, 184: 4259–4267.

[41] R. G. Joshi, D. K. Gupta, P. Amesh, P. K. Parida, and T. R. Ravindran, "Microgel-hydrogel composite photonic crystals to monitor and extract uranyl ions in aqueous solutions," *Microporous Mesoporous Materials*, 2021, 319: 111075.

[42] F. Xiao, Y. Sun, W. Du, W. Shi, Y. Wu, S. Liao, *et al.*, "Smart photonic crystal hydrogel material for uranyl ion monitoring and removal in water," *Advanced Functional Materials*, 2017, 27(42): 1702147.

[43] W. Stöber, A. Fink, and E. Bohn, "Controlled growth of monodisperse silica spheres in the micron size range," *Journal of Colloid Interface Science*, 1968, 26(1): 62–69.

[44] B. Topuz, D. Şimşek, and M. Çiftçioğlu, "Preparation of monodisperse silica spheres and determination of their densification behaviour," *Ceramics International*, 2015, 41(1): 43–52.

[45] R. G. Joshi, B. V. R. Tata, and J. Brijitta, "Pressure tuning of Bragg diffraction in stimuli responsive microgel crystals," *AIP Conference Proceedings, American Institute of Physics*, 2011, 1349(1): 208–209.

[46] J. Brijitta, B. V. R. Tata, R. G. Joshi, and T. Kaliyappan, "Random hcp and fcc structures in thermoresponsive microgel crystals," *Journal of Chemical Physics*, 2009, 131(7): 074904.

[47] D. Karthickeyan, R. G. Joshi, and B. V. R. Tata, "FCC-HCP coexistence in dense thermo-responsive microgel crystals," *Journal of Chemical Physics*, 2017, 146(22): 224503.

[48] M. Stieger, W. Richtering, J. S. Pedersen, and P. Lindner, "Small-angle neutron scattering study of structural changes in temperature sensitive microgel colloids," *Journal of Chemical Physics*, 2004, 120(13): 6197–6206.

[49] G. Lu, A. J. Haes, and T. Z. Forbes, "Detection and identification of solids, surfaces, and solutions of uranium using vibrational spectroscopy," *Coordination Chemistry Reviews*, 2018, 374: 314–344.

[50] A. V. Dubolazov, O. Güven, N. Pekel, G. S. Azhgozhinova, G. A. Mun, and Z. S. Nurkeeva, "Electrochemical, spectroscopic, and thermal studies on interactions of linear poly(acrylic acid) with uranyl ions in aqueous solutions," *Journal of Polymer Science Part B: Polymer Physics*, 2004, 42(9): 1610–1618.

[51] J. Nie, Z. Wang, and Q. Hu, "Chitosan hydrogel structure modulated by metal ions," *Scientific Reports*, 2016, 6(1): 36005.

[52] M. Sivanantham and B. V. R. Tata, "Swelling/ deswelling of polyacrylamide gels in aqueous NaCl solution: light scattering and macroscopic swelling study," *Pramana*, 2012, 79: 457–469.

[53] J. Tan, S. Xie, G. Wang, C. W. Yu, T. Zeng, P. Cai, *et al.*, "Fabrication and optimization of the thermo-sensitive hydrogel carboxymethyl cellulose/poly(N-isopropylacrylamide-co-acrylic acid) for U(VI) removal from aqueous solution," *Polymers (Basel)*, 2020, 12(1): 151.

[54] O. Kharissova, M. Méndez-Rojas, B. Kharisov, U. Méndez, and P. Martínez, "Metal complexes containing natural and artificial radioactive elements and their applications," *Molecules*, 2014, 19(8): 10755–10802.

[55] P. Amesh, A. S. Suneesh, B. R. Selvan, and K. A. Venkatesan, "Amidic succinic acid moiety anchored silica gel for the extraction of UO_2^{2+} from aqueous medium and simulated sea water," *Colloids and Surfaces A: Physicochemical and Engineering Aspects*, 2019, 578: 123585.